Back-analysis of an important sand liquefaction event triggered by the 1870 Charlevoix earthquake, Quebec, Canada

Didier Perret
Natural Resources Canada, Quebec City, Quebec, Canada
Pascal Locat
Ministère des Transports, de la Mobilité Durable et de l'Électrification des Transports, Québec, Québec, Canada
André Pugin
Natural Resources Canada, Ottawa, Ontario, Canada
Antony Gagné
Ministère des Transports, de la Mobilité Durable et de l'Électrification des Transports, Québec, Québec, Canada

ABSTRACT
Unlike high-seismicity regions such as California, Japan or New Zealand, only a few cases of soil liquefaction have been reported historically in the northeastern United States and eastern Canada, where moderate-to-large earthquakes capable of triggering liquefaction are much less frequent. This paper is aimed at documenting one of these liquefaction events, which was triggered in 1870 in the Charlevoix region, Quebec, by an earthquake with a moment magnitude estimated to be in the range 5.8-6.5. Uncertainties in dynamic site response analyses are accounted for by considering four seismic scenarios and several soil resistance profiles obtained from field penetration testing inside and outside the liquefaction zone. For each scenario, synthetic ground motions generated with a stochastic finite-fault model were used to simulate sites response. Results suggest that the most likely scenario for liquefaction triggering was an earthquake with a magnitude of 6.5 at a distance less than or equal to about 10 km.

RÉSUMÉ
À la différence des régions de forte sismicité, comme la Californie, le Japon ou la Nouvelle-Zélande, seuls quelques cas de liquéfaction de sable ont été répertoriés historiquement dans le nord-est des États-Unis et l'est du Canada, où les séismes sont moins fréquents mais peuvent être néanmoins très forts. L'objectif de cette étude est de documenter l'un de ces cas de liquéfaction provoqué en 1870 dans la région de Charlevoix au Québec par un séisme dont la magnitude a été estimée à 5.8-6.5. Les incertitudes dans les analyses de réponse de site sont prises en compte en considérant quatre scénarios sismiques et plusieurs profils de résistance obtenus à l'aide d'essais de pénétration in-situ à l'intérieur et à l'extérieur de la zone affectée par la liquéfaction. Pour chaque scénario, des accélérogrammes synthétiques générés à l'aide d'une méthode stochastique sont utilisés pour simuler la réponse des terrains. Les résultats montrent que le scénario le plus probable ayant provoqué la liquéfaction est un séisme d'une magnitude de 6.5 situé à une distance d'environ 10 km ou moins.

1 INTRODUCTION

Earthquake-induced liquefaction is a phenomenon in which saturated soils, and particularly sands, lose a large part of their strength and stiffness due to pore pressure buildup and behave like a viscous fluid. Liquefaction can lead to ground subsidence, loss of bearing capacity, lateral spreading, and flow slides. Many historical examples show that these seismic-induced settlements and ground failures can result in severe damages to structures, as evidenced for example during the 1964 Niigata, Japan, earthquake (Ishihara and Koga, 1981) and more recently during the Canterbury earthquakes that stroke the Christchurch area in New-Zealand, in 2010 and 2011 (Orense et al., 2011; Potter et al., 2015).

The most up-to-date relations proposed in the literature to discriminate between soils that have liquefied during an earthquake and those that have not are based on case history data that essentially comes from high seismicity regions, such as California, Japan, Turkey, China, and New-Zealand (e.g. Boulanger et al., 2012; Boulanger and Idriss, 2014 and 2015). In the more stable continental areas of eastern North America, moderate-to-strong earthquakes capable of triggering liquefaction are much rarer and none of them are considered in the establishment of the above-cited references. Historically, the largest documented liquefaction event was triggered in 1811-1812 by the New-Madrid, Missouri, earthquake sequence (Obermeier, 1989). Moment magnitudes (M) of the three mainshocks are still a source of controversy. In the last published studies, Hough and Page (2011) estimated that magnitudes ranged from 6.7 to 7.3, but, based on a reinterpretation of eyewitness accounts and felt intensities, Cramer and Boyd (2014) concluded that magnitudes were more likely between 7.3 and 7.7. As per Obermeier (1989), sand blows 30 m in diameter with 1-m-thick ejecta blankets were common in areas where liquefaction was extensive. These sand blow deposits cover over 1% of the ground

surface of an affected area of approximately 230 km × 60 km. Massive sand liquefaction was also triggered in 1886 by the M7.0 Charleston, South-Carolina, earthquake (e.g. Cramer and Boyd, 2014). Sand craterlets as large as 6.4 m in diameter were observed and photographed in the epicentral area. The two other historical earthquakes for which liquefaction phenomena were reported and scientifically analyzed were the 1988 Saguenay, Quebec, earthquake (M5.9; Tuttle et al., 1990) and the 2011 Mineral, Virginia, earthquake (M5.8; Green et al., 2015). Mainly owing to the sparsity of favorable ground conditions, the Mineral earthquake only triggered minor liquefaction close to the epicenter. For the Saguenay earthquake, sand blows and liquefaction dikes were identified within a 30 km radius around the epicenter.

This paper documents another significant case of sand liquefaction in eastern North America, triggered in 1870 in the Charlevoix region, Quebec, by an earthquake whose magnitude has been estimated to be in the range 5.8-6.5. An attempt to better constrain the proposed magnitude range, and to estimate ground motion intensities that led to liquefaction was made by modeling site response for four seismic scenarios.

2 THE 1870 CHARLEVOIX EARTHQUAKE

2.1 Triggering event

The October 20th, 1870 earthquake occurred in the Charlevoix region at about 100 km east of Quebec City, Quebec, in the most active seismic zone of eastern Canada (Fig. 1). It was widely felt, from Nova Scotia in the east to Lake Superior in the west, and to the south, as far as Cincinnati in Ohio, about 1500 km from the epicenter (Lamontagne, 2008). Extensive damage was reported in the epicentral area. According to newspapers reports, several stone-walled houses were destroyed and buildings like churches and flour mills were severely damaged. Most of chimneys were thrown down in Baie-St-Paul, a town with a population of about 3,500 inhabitants in 1870 (Harvey, 2015).

As this earthquake predates the advent of seismographic instrumentation, no recordings are available. Estimates of epicenter location and magnitude are based on the nature and level of damage, on the spatial distribution of damage, and on the extent of the felt area. The Geological survey of Canada (GSC) rates the earthquake magnitude at 6.5 (Lamontagne et al., 2008), based on an important weight given in the estimation to the maximum damages reported in the epicentral area. A reappraisal of newspaper reports and the addition of a few reports not considered before, coupled to a comparative analysis of the impacts of other eastern Canada earthquakes, led Ebel et al. (2013) to propose an intensity magnitude (calibrated to correspond on average to moment magnitude) between 5.5 and 6.0, with a best estimate of 5.8. This is significantly less than the magnitude reported by the GSC. A better consensus exists for the epicenter location, both studies arriving at a similar source area. The epicenter was probably near Baie-St-Paul and the western end of the Coudres Island, where the greatest amount of damage was reported (Fig. 1). Uncertainty in epicenter location is probably no less than about 10 km (J. Ebel, 2015, personal communication).

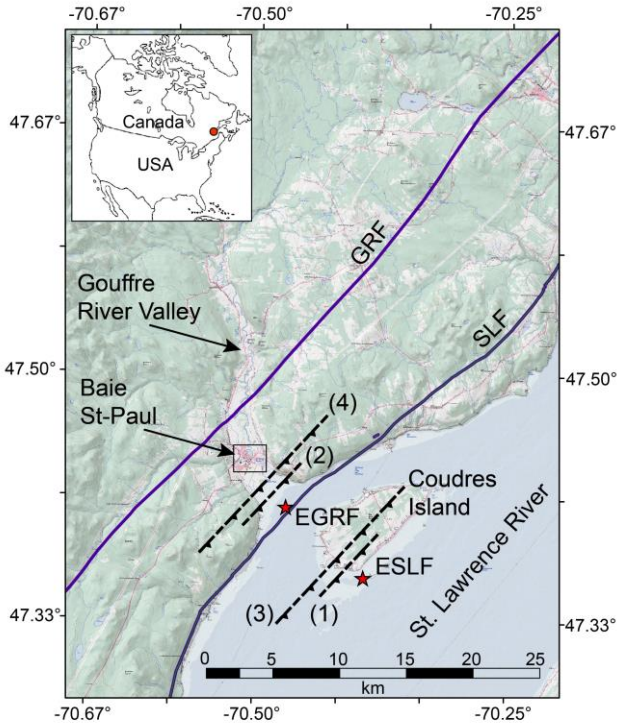

Figure 1. Topographic map of the study area with locations of the St. Lawrence Fault (SLF) and Gouffre River Fault (GRF) traces. Red stars show earthquake epicenters (EGRF and ESLF) associated with SLF and GRF for the four seismic scenarios. Dashed-spiked lines represent the projection at the ground surface of the top of mobilized fault planes. Numbers 1 to 4 refer to seismic scenarios: (1) M5.8-SLF, (2) M5.8-GRF, (3) M6.5-SLF, and (4) M6.5-GRF.

2.2 Liquefaction event

Reliable and unambiguous written accounts by two different people attest that an important liquefaction event occurred in the town of Baie-St-Paul. The first account, by the curate of the parish of Baie-St-Paul, is reported in the ''Journal de Quebec'' of October 22, 1870. An explicit description of what happened is given in this excerpt, translated into English: ''All dwellings seemed to be on a volcano and earth, cracking in five or six places, projected columns of water to six, eight and perhaps fifteen feet in the air, dragging with it a large amount of sand that spilled on the ground''. In the second account published in the ''Journal des Trois-Rivières'' of 24 October 1870, a local police officer mentions that (English translation) ''In several places earth opened, up to ten inches wide, and water came out from the openings with an extraordinary pressure, especially in front of M. Dufour's house where we would have sworn to see a lake. A (*small blacksmith*) shop was engulfed into the ground''. With the help of the Historical Society of Charlevoix (Harvey, 2015), it was

possible to locate with a very good accuracy the area in front of M. Dufour's house, which is the zone where liquefaction was probably the most severe. This zone, hereafter called ZRL (zone of reported liquefaction), is centered at latitude 47.4377°N and longitude 70.5070°W, in the middle of a 3 km wide valley. Its size is difficult to assess but eyewitness accounts along with a reconstitution of the landscape as it was in 1870 suggest a surface area very roughly in the order of 150 m x 150 m.

A small trench excavated in the ZRL, about 2 m deep and 4 m long, found that the ground surface is covered with a thin organic litter, then a sand layer up to about 0.3 m thick, underlain by a silty clay unit about 0.5 m thick followed by a sand deposit. The presence of the surface sand layer is compatible with historical accounts. However, no feeding dikes crossing the silty clay unit were observed, which would have been an unquestionable proof of liquefaction.

3 GEOLOGICAL AND GEOTECHNICAL CHARACTERIZATION

3.1 Subsurface geology

Sediments filling the Gouffre River valley were deposited in a fjord-like environment. A high-resolution seismic reflection line (Pugin et al., 2013) carried out across the valley and the town of Baie-St-Paul shows that the maximum overburden thickness reaches about 300 to 350 m and is about 250 m close to the former house of M. Dufour (Perret, 2012). A simplified stratigraphic log established in a borehole drilled for the groundwater supply of the town about 100 m west of the ZRL center is shown in Fig. 2. The borehole was stopped at a depth of 150 m on a very dense unit consisting in silty sands and cobbles, probably a till or a fluvio-glacial deposit. Sediments from the ground surface down to 150 m were deposited during the late Pleistocene and early Holocene, except perhaps for the first 20 m or so, where they might be more recent. From 150 m down to the bedrock, the nature of soils is uncertain but the analysis of geophysical attributes in the seismic reflection cross-section suggests a succession of coarse sand and gravel units. Considering that rock outcropping on both sides of the valley are the same than those underlying the valley, the bedrock has been inferred to be a limestone of Ordovician age (Rondot, 1979).

The sand unit that was affected by liquefaction varies in thickness from 2 m in the western part of the ZRL to 21 m in its eastern part. These sands have a deltaic origin and were transported over a short distance by a fluvial stream and possibly reworked in a coastal environment. Rapid lateral variations in thickness in the ZRL, and in facies in the valley around Baie-St-Paul (from sands to clays) may indicate, however, that these deposits were the result of early Holocene submarine landslides or of a basin collapse induced by the ~M7.5 1663 Charlevoix earthquake (Fillion et al., 1991; Ebel, 2011).

3.2 Geotechnical characterization

A composite shear wave velocity profile representative of the ZRL (red line, Fig. 2), was constructed from seismic cone penetration tests (SCPT) and the high-resolution seismic reflection survey. SCPT values were used to establish the profile down to 50 m, the greatest depth reached by these tests. The values extracted from the seismic reflection cross-section were used at larger depths. The energy and frequency content delivered by the shaker truck employed for the seismic reflection survey (Pugin et al., 2013) did not allow for a penetration greater than 150 m in S-wave mode, the energy being almost entirely reflected on top of the very dense unit containing cobbles. The few erratic S-wave velocities determined at greater depths were judged unreliable and are not plotted in Fig. 3. The time-averaged shear wave velocity in the first 30 m, Vs_{30}, is 210 m/s for the profile representative of the ZRL. Empirical correlations based on penetration resistance and shear wave velocity were used to estimate unit weights.

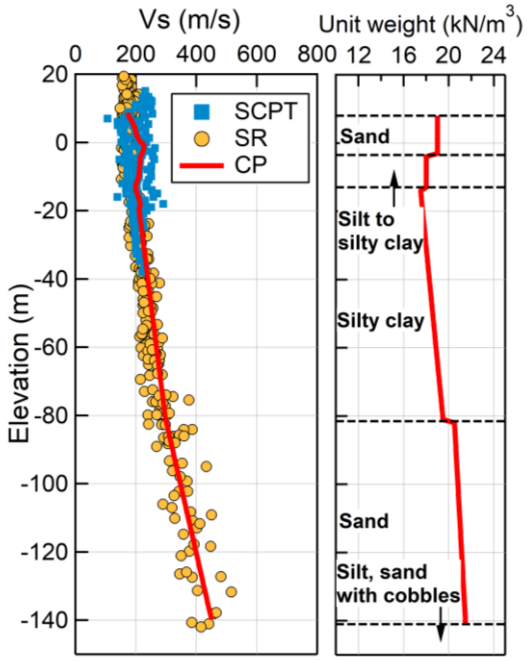

Figure 2. Shear wave velocity and unit weight profiles with simplified stratigraphic log (SCPT: seismic cone penetration tests, SR: seismic reflection survey, CP: composite profile). Elevation at ZRL center is 9 m asl.

Six cone penetration tests (CPT) and seven standard penetration tests (SPT) were performed inside the ZRL. To illustrate the properties and variability over short distances of investigated soils, Fig. 3a shows depth profiles for four CPTs and two SPTs located within a radius of 25 m from the ZRL center. Both SPT and CPT profiles follow the same trends, but a larger scatter is observed between N values profiles than between q_t values profiles at certain depths. From one to 13 m, the deposit is a medium dense to dense sand, with a D_{50} of about 0.2-0.5 mm and a fines content varying between 3 and 12%. The underlaying unit is a homogeneous silty clay of medium to high sensitivity with a plasticity index of 30-40 and an over-consolidation ratio (OCR) of about 1.3-2.5, sometimes interbedded with thin sand layers. Normalized soil behavior type (SBTn) indices Ic are plotted in Fig. 3b. As already shown for eastern

Canada sands (Perret et al., 2016), a good correlation was observed here too between Ic and fines content.

In addition to a few sites specifically characterized outside the ZRL for this study, we also had access to the results of several other geotechnical investigations conducted in the last ten years in Baie-St-Paul for the construction of a hospital and the seismic retrofitting of buildings. Some of these geotechnical profiles, obtained in the same geological context but where no evidence of past liquefaction was found or documented historically, were analyzed for comparison.

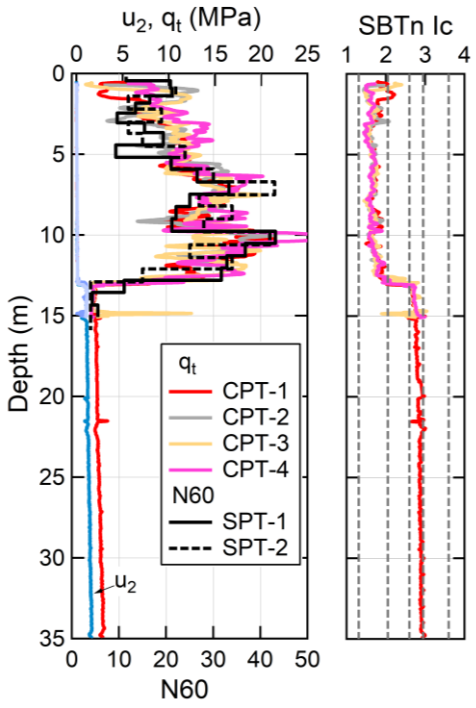

Figure 3. SCPT and SPT profiles near the ZRL center (SBPTn Ic: Normalized Soil Behavior Type Index). Vertical dashed lines on the right plot correspond to Ic cut-offs used for soil classification as defined in Robertson (2009).

4 METHODOLOGY

4.1 Cyclic stress procedure for liquefaction potential assessment

The most widely used method to assess the potential for liquefaction triggering, or for simplicity, the liquefaction potential, is based on the site-specific, cyclic stress procedure devised by Seed and Idriss (1971) and Whitman (1971). In this procedure, which was refined several times since its formulation (see e.g. Youd et al., 2001, and Boulanger and Idriss, 2014), the factor of safety against liquefaction triggering is given by the ratio of the liquefaction resistance of the soil to the cyclic loading generated at the site of interest by an earthquake. Liquefaction resistance is characterized by the cyclic resistance ratio (CRR) and is typically obtained from in-situ penetration testing, like SPTs and CPTs. Seismic loading is defined by the cyclic shear stress ratio (CSR) and is expressed in the rigorous approach as:

$$\mathrm{CSR} = 0.65\ \frac{\tau_{max}}{\sigma'_{v0}} \qquad [1]$$

where τ_{max} is the total, maximum horizontal cyclic shear stress imposed at a given depth by earthquake loading, σ'_{v0}, the vertical effective stress due to overburden, and 0.65, a coefficient introduced to account for the effect of stress cycles with different amplitudes in a ground motion time history. In the rigorous approach site-specific dynamic response analyses are performed to compute shear stresses, usually for one-dimensional (1-D) conditions. Calculations require knowledge of the soil's physical properties, the shear wave velocity profile, and the shear modulus degradation and damping curves for each soil. Ground motion time series representative of the reference site conditions are also required to perform analyses. In the simplified approach, shear stresses are approximated from horizontal peak ground accelerations at the site surface, a_{max}, modulated at each depth by a shear stress reduction coefficient r_d accounting for flexibility of the soil column:

$$\mathrm{CSR} = 0.65\ \frac{\sigma_{v0}}{\sigma'_{v0}}\ \frac{a_{max}}{g}\ r_d \qquad [2]$$

where g is the acceleration of gravity, and σ_{v0} the total vertical overburden stress. In deterministic analyses, the peak ground acceleration at the surface is generally obtained by multiplying the peak ground acceleration given by a ground motion prediction equation (GMPE) for a reference site condition and a specific magnitude-distance scenario, with an amplification factor depending on site characteristics and shaking intensity (see e.g. Kramer, 2008). For both procedures, normalizing factors are applied to the CSR or CRR to account for the number of cycles in a time series and the influence of confining pressure.

In the method developed by Green et al. (2005) for the backward analysis of past liquefaction events for which the ground motion characteristics and magnitudes are unknown, the CSRs corresponding to a safety factor of 1.0 are calculated with the simplified approach for several seismic scenarios each represented by a (a_{max}, M) pair. The most likely scenario which led to liquefaction at a given site is then determined by comparison of the values calculated from a GMPE for different site-to-source distances and magnitudes. Amplification factors representative of the soils and of the seismological environment in the region where liquefaction occurred must be available to obtain reliable results. As factors tailored for Eastern Canada conditions have not yet been developed, it was deemed preferable to use the rigorous approach and to carry out dynamic site response analyses instead of applying factors developed for other environments with unproven representativeness or for forward analyses like in NBCC (2015).

For the estimation of the liquefaction potential, normalized CSR and CRR were determined with the most up-to-date relations developed by Boulanger and Idriss (2014, 2015). Only CPT data were considered in this

preliminary study as they were judged more reliable than SPT data.

4.2 Estimation of liquefaction severity

The factor of safety against liquefaction triggering provides a quantitative estimation of the ability of a soil layer to resist liquefaction. However, this parameter does not inform on the overall behavior of a soil deposit and on the consequences of liquefaction. The liquefaction severity number (LSN) recently proposed by van Ballegooy et al. (2014) was adopted in this study to assess the severity of liquefaction manifested at the ground surface. This index is defined as the summation of the post-liquefaction volumetric reconsolidation strains calculated for each soil layer divided by the depth of that layer:

$$\mathrm{LSN} = 10 \int_0^{LD} \frac{\varepsilon_v}{z} dz \qquad [3]$$

where ε_v is the volumetric strain in percent, z, the depth in meter, and LD, the limiting depth over which the index is calculated, taken at 10 m below the ground surface as recommended in Tonkin and Taylor (2015). Based mainly on the performance of residential buildings during the Christchurch earthquake sequence, the following threshold values have been proposed to rank liquefaction severity (NZGS, 2016):

- $\mathrm{LSN} < 10$: Insignificant
- $5 < \mathrm{LSN} < 15$: Mild
- $10 < \mathrm{LSN} < 25$: Moderate
- $15 < \mathrm{LSN} < 35$: High
- $\mathrm{LSN} > 30$: Severe

The reader is referred to van Ballegooy et al. (2014), Tonkin and Taylor (2015), and NZGS (2016) for a justification of using the LSN over other indicators as well as for a detailed description of impact ranking.

4.3 Seismic scenarios

It has been shown that in the Charlevoix region, hypocenters of earthquakes with magnitudes greater than 4.0 tend to align along two main faults parallel to the St. Lawrence River, steeply dipping to the southeast (Lamontagne and Ranalli, 2014; Yu et al., 2016). The surface traces of these faults, the St. Lawrence Fault (SLF) and the Gouffre River Fault (GRF), are indicated in Fig. 1, as identified by Rondot (1979). Knowing that the epicenter of the 1870 earthquake was likely near the western end of the Coudres Island, it is reasonable, in the absence of other information, to speculate that this earthquake was initiated along one of these two faults. To cover the estimated magnitude range proposed for the 1870 earthquake, four seismic scenarios were considered: two earthquakes with M5.8 and M6.5 for each of the two faults.

Synthetic ground motions were generated for each of these scenarios with code EXSIM implemented in the Southern California Earthquake Center Broadband Platform (SCEC-BBP, release v17.3; Atkinson and Assatourians, 2015; Maechling et al., 2015). Code EXSIM, initially developed by Motazedian and Atkinson (2005), is based on a stochastic extended finite-fault algorithm that simulates ground motion time series. A fault plane with dimensions consistent with the magnitude of the earthquake to be modelled is divided into subfaults, each considered as a stochastic point-source generating a ground motion. At the site of interest located at a given distance from the fault, ground motions emanating from subfaults are summed to obtain a time series representative of the entire modeled fault. Input parameters to fix source, subsource, and propagation characteristics were those defined for central and eastern North America in Atkinson and Assatourians (2015).

Fault sizes were estimated from relations presented in Leonard (2010) for stable continental regions. For M 5.8 and 6.5, the fault widths and lengths are respectively, 4.7 km and 6.4 km, and 8.0 km and 14.3 km. Faults have the same strike (42º), rake (105º), and dip (53º to the southeast) than the M6.2 1925 Charlevoix earthquake taken here as reference (Bent, 1992). Focal depth is set at 10 km in the center of the fault plane for the four scenarios, this depth corresponding to the depth where most seismic events cluster beneath the Coudres Island (Yu et al., 2016). The Joyner-Boore distances (defined as the shortest horizontal distance from the ZRL center to the surface projection of the rupture surface), are respectively, 10.6 km and 9.6 km for the M5.8-SLF and M6.5-SLF scenarios, and 2.8 km and 1.8 km for the M5.8-GRF and M6.5-GRF scenarios.

For each scenario, one-hundred time series were computed, each realization adopting random slips to account for uncertainties in fault movement.

4.4 Dynamic site response analyses

To determine shear stresses induced in the soil column (Fig. 2) by the synthetic ground motions, both total stress equivalent-linear (EL) and nonlinear (NL) 1-D dynamic site response analyses were performed with the computer program DEEPSOIL (Hashash et al., 2018). Shear modulus degradation and damping curves were obtained from relationships developed by Darendeli (2001). These curves were modified by applying the DS-EL4/DS-NL4 models so that the implied shear strengths were consistent with the soil shear strengths at large strains (General Quadratic/Hyperbolic model with non Masing rules). For clays, shear strengths were determined by using a constant $Su/(OCR \times \sigma'_{v0})$ ratio equal to 0.25 and an average OCR = 1.75, while for coarse-grained soils, a unique friction angle of 37º and an OCR = 1.0 were considered. To account for strain rate effects in clays, static shear strengths were multiplied by 1.4, assuming that these effects were not compensated by possible cyclic softening effects (Lefebvre and Pfendler, 1996; Stewart et al., 2014). No strain-rate correction was applied for coarse-grained soils. For comparison, simulations were also performed without strain rate effects for both clays and sands. If not specified otherwise, the results presented will be for simulations considering strain rate effects in clays. The soil profile was discretized so that the maximum propagated frequency was at least about 40 Hz. All other parameters

needed for modeling were those recommended in DEEPSOIL.

Input ground motions were applied at a depth of 150 m, on top of the very dense unit with cobbles. Had the bedrock been selected, additional uncertainties would have been introduced into the modeling, since the shear wave velocity profile should have been extrapolated over a hundred meters with few constraints. This choice is supported by ambient noise measurements which indicate that the fundamental period at the ZRL center is 1.8 s (Perret, 2012), a value almost identical to the fundamental period calculated from the shear wave velocity profile of Fig.2 with a plane-wave propagation algorithm. This means that the interface controlling the main resonance is located at a depth of 150 m, which seems logical considering the nature of the soils at this depth. Shear wave velocity of the half-space has been set at 1000 m/s.

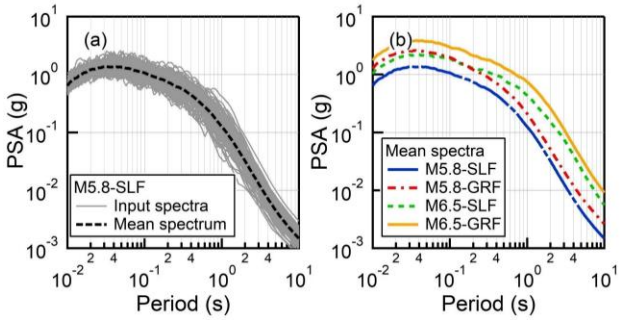

Figure 4. (a) Response spectra of the one-hundred synthetic ground motions for seismic scenario M5.8-SLF, and (b) geometric means of response spectra for the four seismic scenarios.

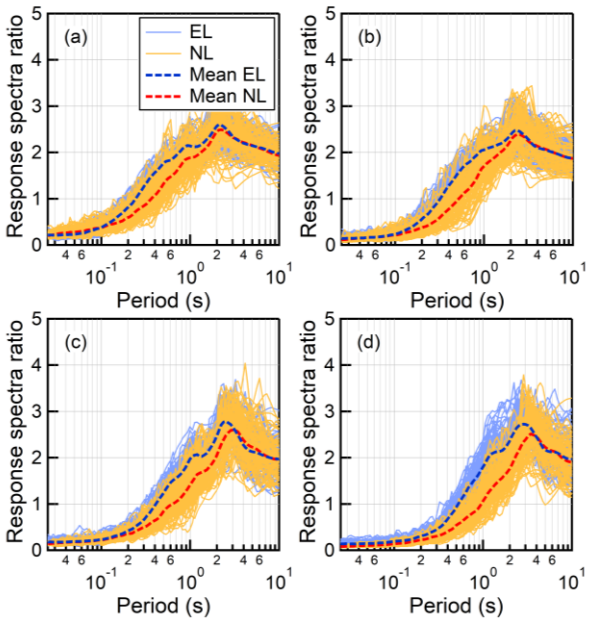

Figure 5. Ratios of surface response spectra to input response spectra (EL: equivalent-linear, NL: nonlinear) for the four seismic scenarios: (a) M5.8-SLF, (b) M5.8-GRF, (c) M6.5-SLF, and (d) M6.5-GRF.

5 RESULTS

5.1 Spectral accelerations

Simulated fault planes being close to the ZRL center, input ground motions generated with code EXSIM are characterized by high spectral accelerations, with peak ground accelerations up to about 2 g for the scenario M6.5-GRF. Figure 4 shows response spectra at the ZRL center for a fictitious outcropping site with a shear wave velocity Vs_{30} = 1000 m/s. In Fig. 4a, response spectra corresponding to scenario M5.8-SLF are shown for the one-hundred realizations to illustrate the typical ground motion variability considered within a given scenario. Mean response spectra for the four scenarios are shown in Fig. 4b. At periods between 0.1 and 1 s, spectral accelerations vary by a factor of almost six for the two extreme scenarios (M5.8-SLF vs M6.5-GRF). For periods longer than 0.4 s, the location of the rupture surface with respect to the site has a relatively minor effect, the variation being essentially due to the magnitude difference.

Surface response spectra exhibit important deamplification at periods shorter than 0.2-0.4 s, for both EL and NL analyses (Fig. 5). The ratios between the surface and input response spectra are well below one, indicating that seismic energy is strongly dissipated for short periods during wave propagation in the soil column. On average, the maximum amplification is about 2.5-2.7, with slightly lower values observed for NL analyses. This maximum occurs at periods longer than the fundamental site period (1.8 s) reflecting a decrease in soil rigidity.

5.2 Liquefaction potential and severity

Profiles of fully adjusted CSR (CSR*) and CRR (CRR*) accounting for magnitude, confining pressure, and fines content effects, are shown in Figure 6 for a CPT close to the ZRL center. A liquefaction probability of 15% was considered, as recommended by Boulanger and Idriss (2015) for deterministic analyses. The groundwater table was set at a depth of 1 m, a plausible level for late October, the period during which the 1870 earthquake occurred. CSR* values in Figure 6 were calculated for clays with dynamic shear strengths that are 40% higher than static shear strengths (see section 4.3). Difference with modeling performed with no strain rate effects is negligible except for the strongest events considered (M6.5-SLF and M6.5-GRF), for which CSR are, at the maximum, about 15% lower in the first 13 m. As it did not change the overall picture, results for the no-strain-rate-effect condition are not presented.

It is noteworthy that CSR* resulting from NL modeling are systematically and significantly lower than those obtained from EL modeling. For NL analyses, the liquefaction potential is found to be inexistent or marginal for scenarios M5.8-SLF, M5.8-GRF and M6.5-SLF (Fig. 6a,b,e). Only the scenario M6.5-GRF (Fig. 6f) could trigger significant liquefaction at depths between 1.0 and 2.5 m and 11.6 to 12.6 m where CSR* are greater than CRR*. For the M6.5-GRF scenario, the LSN is about 24 indicating a moderate to high liquefaction severity.

Results from EL analyses give a different portrait. The liquefaction potential becomes high beginning with scenario M5.8-GRF for which the LSN is 29, with the possibility to have important surface expressions of liquefaction. Scenarios M6.5-SLF and M6.5-GRF (Fig. 6g,h) are respectively characterized by LSN of 35 and 39. This range of values has been associated with severe liquefaction developing in most of the deposit (NZGS, 2016).

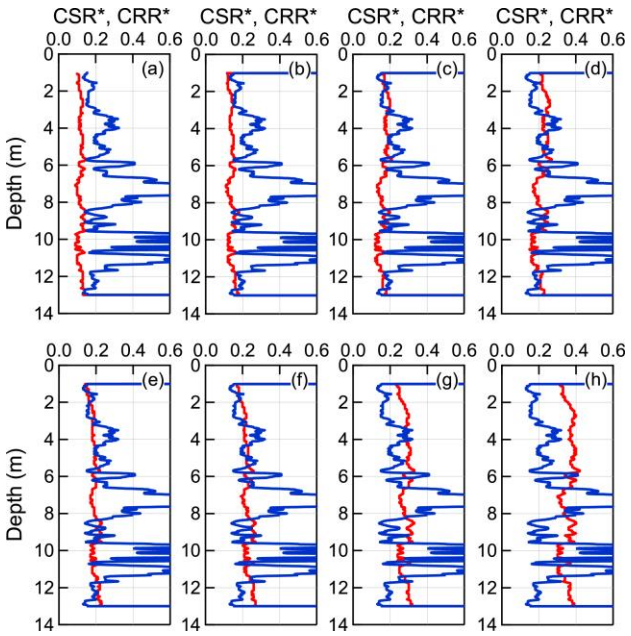

Figure 6. Profiles of fully adjusted CSR (in red, CSR*) and CRR (in blue, CRR*) for CPT-1 shown in Figure 3. Profiles are presented for equivalent-linear (EL) and nonlinear (NL) modeling and for the four seismic scenarios: (a) NL M5.8-SLF, (b) NL M5.8-GRF, (c) EL M5.8-SLF, (d) EL M5.8-GRF, (e) NL M6.5-SLF, (f) NL M6.5-GRF, (g) EL M6.5-SLF, and (h) EL M6.5-GRF.

Critical layers that may have contributed the most to the surface manifestation of liquefaction (sand ejecta and settlements) are close to the ground surface, probably in the first 3 m and not deeper than about 5.5 m. Deeper layers showing liquefaction at 8.0-9.5 m and 11.6-12.6 m are overlain by much denser sand layers 1 and 2 m thick and it is doubtful that sands from these depths would have gone through the deposit to the ground surface. This is supported by the arguments considered in the formulation of the LSN and in setting the limiting depth at 10 m (Eq. 3; van Ballegooy et al., 2014).

Figure 7 shows, for the four seismic scenarios, the distributions of LSN values calculated from CPT profiles obtained inside and outside the ZRL. Three CPTs from the area outside the ZRL were on the same terrace and at the same elevation (about 8-10 m) than those inside the ZRL. The eleven other CPTs outside the ZRL were performed on a higher terrace located about 200 m away from the ZRL at an elevation of about 12-15 m. On this terrace, soils in the first three to five meters below the ground surface are a mixture of sands, gravels, and boulders, deposited by a tributary of the Gouffre River probably during torrential floods. At greater depths, the stratigraphy is like what is observed close to the ZRL center (Fig. 2). All selected CPT profiles comprise a sand unit down to a depth of at least 10 m. It was assumed that CPT sites are close enough to the ZRL center to apply the CSR profiles calculated with profiles shown in Fig.2 to each one of these sites.

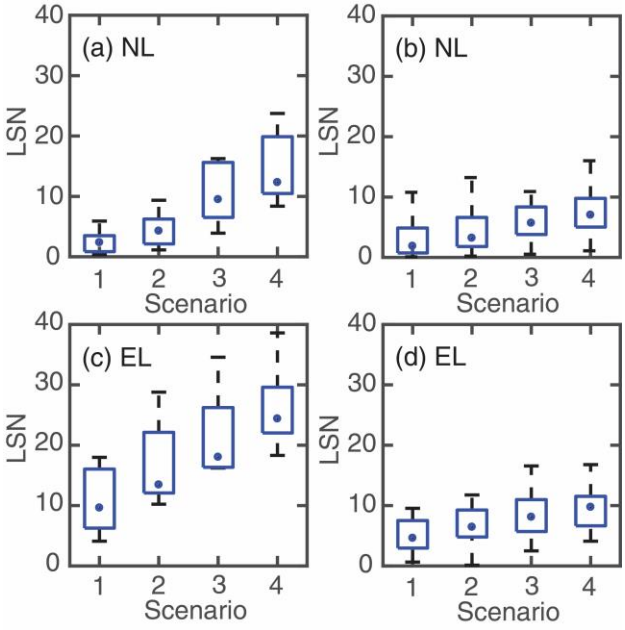

Figure 7. Box and whisker plots showing the distribution of liquefaction severity numbers (LSN) calculated from CPT profiles inside (a, c) and outside (b, d) the ZRL, for the four seismic scenarios: (1) M5.8-SLF, (2) M5.8-GRF, (3) M6.5-SLF, and (4) M6.6-GRF. Dots correspond to median values, and the bottom and top of boxes to the 25 and 75 percentiles of distributions, respectively. Whiskers extend to the highest and lowest calculated values.

For CPT profiles inside the ZRL, the liquefaction severity increases with earthquake magnitude and decreases with distance to the ruptured fault. Median values for NL analyses (Fig. 7a) are lower than 15 even for the strongest event modeled, which means that mild to moderate liquefaction manifestations could be expected at the ground surface. Distribution for the M6.5-GRF event is, however, strongly skewed towards high values, with LSN values up to 25. The fact that the highest LSN values calculated for M5.8 scenarios are less than 10 and that M6.5 scenarios are characterized by values capable of generating surface manifestations of liquefaction, suggests that a M6.5 scenario is much more likely for the 1870 earthquake. The distributions for EL analyses (Fig. 7c) are wider and shifted to higher values relative to NL analyses. It is more difficult to dissociate scenarios based on magnitude, the overlap between distributions being important. According to EL analyses, scenarios 2 to 4 could be plausible candidates for the 1870 earthquake.

The LSN values are much less variable for profiles outside the ZRL, irrespective of the scenario (Fig. 7b,d).

With median values not higher than 10 for both EL and NL analyses, expected surface manifestation of liquefaction is insignificant or mild at best. Low LSN values result from the presence above sand deposits, of the dense unit with gravels and boulders, which was assumed non-liquefiable in analyses due to its nature and because the water table on the higher terrace was probably three to five meters deeper than in the ZRL at the time of the 1870 earthquake, as observed today. Although the absence of evidence is not evidence of absence, these results may explain why significant liquefaction manifestations were not reported in historical accounts outside the ZRL.

6 DISCUSSIONS AND CONCLUSIONS

Several simplifying assumptions as well as arbitrary choices were made in simulating ground motions. Seismic scenarios were based on best possible estimates, but uncertainties remain in the ruptured fault location and dimensions, and in the earthquake focal depth, which were not accounted for in simulations. For example, a shallower earthquake would have generated stronger accelerations whereas the opposite would have been observed for a ruptured fault location further away from the ZRL. Although EXSIM code as implemented in the SCEC-BBP has been successfully validated for some earthquakes in North America and in Japan (Atkinson and Assatourians, 2015), near-field effects that may modify ground motion characteristics close to a fault, like the generation of a strong velocity pulse due to directivity effects, are not specifically modeled. Similar comments can be made for site response analyses. Soil shear modulus degradation and damping curves were established based on Darendeli's (2001) work only, without knowing whether these curves adequately represent the behavior of the investigated soils. In addition, no relationships other than those developed by Boulanger and Idriss (2015) were used to estimate the liquefaction potential. Another assumption made in this study is that site response can be realistically assessed from 1-D modeling. A better appraisal of ground motion and soil response variability due to these epistemic uncertainties could have been obtained by conducting exhaustive sensitivity analyses, and by considering other fault rupture simulation codes (see e.g. Maechling et al., 2015) but it was beyond the scope of this preliminary study.

It has been implicitly assumed that the current soil resistance as determined by in-situ penetration tests is representative of the situation prevailing before the 1870 earthquake occurred, which is a strong hypothesis requiring some explanations. Sand ejecta and ground settlements induced by liquefaction can be seen in a first analysis as leading to densification and to an increase in soil liquefaction resistance. This cannot be excluded in some circumstances, but numerous observations indicate to the contrary that soils that once liquefied can liquefy again, even under lower ground motion intensities and with even greater manifestations at the ground surface (e.g. Ishihara and Koga, 1981; Obermeier, 1989; Sims and Garvin, 1995; Orense et al., 2011; NZGS, 2016). Liquefaction is a complex phenomenon during which inhomogeneities and weaknesses are created in a soil deposit. Buildup of pore pressure may result in pore water migration to upper layers and a decrease in resistance in these layers. It would be surprising that sites investigated in the ZRL would have been affected in the same manner during the 1870 earthquake with sites all showing either densification or loosening relative to pre-earthquake conditions. On average, CPT profiles can probably be confidently used to evaluate site performance during the simulated earthquakes.

The important difference noticed between results obtained from EL and NL analyses has direct implications on the interpretation of LSN values and consequently on the determination of the seismic scenario that best explains the 1870 earthquake ground surface liquefaction manifestations. EL analyses consistently give higher LSN values, and the question arises as to which site response modeling method would give the best interpretation. It has been shown that both methods give similar results for low level accelerations for which induced shear strains are not too high. In situations characterized by high input spectral accelerations like those modeled in this study, large shear strains are generated, and it is generally admitted that nonlinear modeling allows for a more accurate representation of the cyclic stress-strain behavior of soils (e.g. Kaklamanos et al., 2013; Stewart et al., 2014). Accordingly, results presented in Fig. 7a for NL analyses would be preferred in this situation.

Historical accounts describe important liquefaction manifestation at the ground surface (sand and water geysers, a small blacksmith shop sinking into the ground). LSN values calculated from NL analyses rather indicate mild to moderate impacts based on the thresholds defined by NZGS (2016). This apparent contradiction can be reconciliated by recalling that historical accounts were certainly biased, with only the most remarkable and intriguing impacts being reported. In addition, the thresholds in NZGS (2016) were mainly established from the performance of residential buildings, and not on the direct assessment of the magnitude of liquefaction manifestation at the ground surface in the absence of structures, although there is an obvious correlation between the two.

This preliminary study did not provide a clear-cut answer as to which scenario was responsible of the 1870 liquefaction event. However, a careful interpretation of the results of 1-D site response analyses suggests that an earthquake with a moment magnitude of 6.5 at a distance less than or equal to about 10 km is the most likely scenario for liquefaction triggering. A M5.8 scenario, as modeled, appears to not be able to trigger significant liquefaction. In a second phase of this study, sensitivity analyses and 2-D modeling of the Baie-St-Paul basin will be performed to confirm or contradict these conclusions.

ACKNOWLEDGEMENTS

This study was supported by the Public Safety Geoscience Program, Land and Minerals Sector, Natural Resources Canada, and represents LMS Contribution 20180121. The authors would like to thank Transports Québec, the Charlevoix School Board, the Charlevoix Health and Social Service Center, and the municipality of Baie-St-Paul, for the permission to use geotechnical data. The authors also

wish to thank Maurice Lamontagne for the review of a draft of this paper.

REFERENCES

Atkinson, G.M. and Assatourians, K. 2015. Implementation and validation of EXSIM (A Stochastic Finite-Fault Ground-Motion Simulation Algorithm) on the SCEC Broadband Platform. *Seismological Research Letters*, 86(1):48-60, doi:10.1785/0220140097.

Bent, A.L. 1992. A re-examination of the 1925 Charlevoix, Québec, earthquake. *Bulletin of the Seismological Society of America*, 82(5):2097-2113.

Boulanger, R.W., Wilson, D.W. and Idriss, I.M. 2012. Examination and reevaluation of SPT-based liquefaction triggering case histories. *Journal of Geotechnical and Geoenvironmental Engineering*, ASCE, 138(8):898-909.

Boulanger, R.W. and Idriss, I.M. 2014. CPT and SPT based liquefaction triggering procedures. *Report UCD-CGM-14/01, Department of Civil and Environmental Engineering*, University of California at Davis, 138 pp.

Boulanger, R.W. and Idriss, I.M. 2015. CPT-based liquefaction triggering procedure. *Journal of Geotechnical and Geoenvironmental Engineering*, ASCE, 142(2):04015065-1.

Cramer, C.H. and Boyd, O.S. 2014. Why the New Madrid earthquakes are M 7-8 and the Charleston earthquake is ~M 7. *Bulletin of the Seismological Society of America*, 104(6):2884-2903.

Darendeli, M.B. 2001. Development of a new family of normalized modulus reduction and material damping curves. *Department of Civil Engineering*, University of Texas, Austin, TX, 395 pp.

Ebel, J.E. 2011. A new analysis of the magnitude of the February 1663 earthquake at Charlevoix, Quebec. *Bulletin of the Seismological Society of America*, 101(3):1024-1038.

Ebel, J.E., Dupuy, M. and Bakun, W.H. 2013. Assessing the location and magnitude of the 20 October 1870 Charlevoix, Quebec, earthquake. *Bulletin of the Seismological Society of America*, 103(1):588-594.

Fillion, L., Quinty, F. and Bégin, C. 1991. A chronology of landslide activity in the valley of Rivière du Gouffre, Charlevoix, Quebec. *Canadian Journal of Earth Sciences*, 28:250-256.

Green, R.A., Obermeier, S.F. and Olson, S.M. 2005. Engineering geologic and geotechnical analysis of paleoseismic shaking using liquefaction effects: field examples. *Engineering Geology*, 76:263-293.

Green, R.A., Lasley, S., Carter, M.W., Munsey, J.W., Maurer, B.W. and Tuttle, M.P. 2015. Geotechnical aspects in the epicentral region of the 2011 M 5.8 Mineral, Virginia, earthquake. *Geological Society of America,* Special Paper 509, p. 151-172.

Harvey, C. 2015. Earthquakes in Charlevoix according to historical documents (in French). *Edition Charlevoix,* Société d'histoire de Charlevoix, 123 pp.

Hashash, Y.M.A., Musgrove, M.I., Harmon, J.A., Groholski, D.R., Phillips, C.A. and Park, D. 2018. DEEPSOIL 7.0, User Manual. *Urbana, IL, Board of Trustees of University of Illinois at Urbana-Champaign*, 169 pp.

Hough, S.E. and Page, M. 2011. Toward a consistent model for strain accrual and release for the New Madrid seismic zone, central United States. Journal of Geophysical Research, B03311, 10.1029/2010JB 007783.

Ishihara, K. and Koga, Y. 1981. Case studies of liquefaction in the 1964 Niigata earthquake. *Soils and Foundations*, 21(3):35-52.

Kaklamanos, J., Bradley, B.A., Thompson, E.M. and Baise, L.G. 2013. Critical parameters affecting bias and variability in site-response analyses using KiK-net downhole array data. *Bulletin of the Seismological Society of America*, 103 (3):1733-1749.

Kramer, S.L. 2008. Evaluation of liquefaction hazards in Washington State. *Final Research Report WA-RD 668.1,* Washington State Department of Transportation, 329 pp.

Lamontagne, M. 2008. Casualties directly caused by an earthquake in Canada: First contemporaneous written accounts from the M6.5 Charlevoix, Quebec, earthquake of 20 October 1870. *Bulletin of the Seismological Society of America*, 98(3):1602-1606.

Lamontagne, M., Halchuk, S., Cassidy, J.F. and Rogers, G.C. 2008. Significant Canadian earthquakes of the period 1600–2006, *Seismological Research Letters*, 79:211–223.

Lamontagne, M. and Ranalli, G. 2014. Earthquakes and geological structures of the St. Lawrence rift system. In *Intraplate Earthquakes,* P. Talwani (Ed.), Chap. 4, Cambridge University Press, New York, 398 pp.

Lefebvre, G. and Pfendler, P. 1996. Strain rate and preshear effects in cyclic resistance of soft clay. *Journal of Geotechnical and Geoenvironmental Engineering*, ASCE, 122(1):21-26.

Leonard, M. 2010. Earthquake fault scaling: Self-consistent relating of rupture length, width, average displacement, and moment release. *Bulletin of the Seismological Society of America*, 100(5A):1971-1988.

Maechling, P.J., Silva, F., Callaghan, S. and Jordan, T.H. 2015. SCEC Broadband Platform: System Architecture and Software Implementation, *Seismological Research Letters*, 86(1), doi: 10.1785/0220140125.

Motazedian, D. and Atkinson, G.M. 2005. Stochastic finite-fault model based on dynamic corner frequency. *Bulletin of the Seismological Society of America*, 95(3): 995-1000.

NBCC 2015. National building code of Canada. *Canadian Commission on Building and Fire Codes*, National Research Council Canada.

NZGS 2016. Earthquake geotechnical engineering practice, Module 3: Identification, assessment and mitigation of liquefaction hazards. *New Zealand Geotechnical Society, Wellington (NZ):* Ministry for Business, Innovation and Employment, 44 pp.

Obermeier, S.F. 1989. The New Madrid earthquakes—an engineering–geologic interpretation of relict liquefaction features. *U.S. Geological Survey,* Professional Paper 1336-B, 114 pp.

Orense, R.P., Kiyota, T., Yamada, S., Cubrinovski, M., Hosono, Y., Okamura, M. and Yasdu, S. 2011. Comparison of liquefaction features observed during

the 2010 and 2011 Canterbury earthquakes. *Seismological Research Letters*, 82(6):905-918.

Perret, D., 2012. Single station H/V technique. In Shear Wave Velocity Measurement Guidelines for Canadian Seismic Site Characterization in Soil and Rock, (ed.) J.A. Hunter and H.L. Crow, *Geological Survey of Canada*, Open File 7078, p. 78-84.

Perret, D., Charrois, E. and Bolduc, M., 2016. Shear wave velocity estimation from piezocone test data for Eastern Canada sands (Quebec and Ontario) – Extended version with appendices. *Geological Survey of Canada,* Open File 8121, 47 pp.

Potter, S.H., Becker, J.S., Johnston, D.M. and Rossiter, K.P. 2015. An overview of the impacts of the 2010-2011 Canterbury earthquakes. *International Journal of Disaster Risk Reduction*, 14:6-14.

Pugin, A.J.M., Brewer, K., Cartwright, T., Pullan, S.E., Perret, D., Crow, H. and Hunter, J.A. 2013. Near surface S-wave seismic reflection profiling – New approaches and insights. *First Break*, 31(2):49-60.

Robertson, P.K. 2009. Interpretation of cone penetration tests – a unified approach. Canadian Geotechnical Journal, 46:1337-1355.

Rondot, J. 1979. Reconnaissances géologiques dans Charlevoix-Saguenay. *Rapport DPV-682*, Ministère des richesses naturelles du Québec, 51 pp.

Seed, H.B and Idriss, I.M. 1971. Simplified procedure for evaluating soil liquefaction potential. *Journal of the Soil Mechanics and Foundations Division*, ASCE, 97(9): 1249-1273.

Sims, J.D. and Garvin, C.D. 1995. Recurrent liquefaction induced by the 1989 Loma Prieta earthquake and 1990 and 1991 aftershocks: Implications for paleoseismicity studies. *Bulletin of the Seismological Society of Americ*a, 85(1):51-65.

Stewart, J.P., Afshari, K. and Hashash, Y.M.A. 2014. Guidelines for performing hazard-consistent one-dimensional ground response analysis for ground motion prediction. *Report PEER 2014-16,* Pacific Earthquake Engineering Research Center, 152 pp.

Tonkin & Taylor 2015. Canterbury earthquake sequence: Liquefaction vulnerability assessment methodology. *Tonkin & Taylor Ltd., Project Number 52010.140.v1.0*, 204 pp. + Appendices.

Tuttle, M., Law, K.T, Seeber, L. and Jacob, K. 1990. Liquefaction and ground failure induced by the 1988 Saguenay, Quebec, earthquake. *Canadian Geotechnical Journal*, 27:580-589.

van Ballegooy, S., Malan, P., Lacrosse, V., Jacka, M.E., Cubrinovski, M., Bray, J.D., O'Rourke, T.D., Crawford, S.A. and Cowan, H. 2014. Assessment of liquefaction-induced land damage for residential Christchurch. *Earthquake Spectra*, 30(1):31-55.

Whitman, R.V. 1971. Resistance of soil to liquefaction and settlement. *Soils and Foundations*, 11(4):59-68.

Youd, T.L. et al. 2001. Liquefaction resistance of soils: summary report from the 1996 NCEER and 1998 NCEER/NSF workshops on evaluation of liquefaction resistance of soils. *Journal of Geotechnical and Geoenvironmental Engineering*, ASCE, 127(10):817-833.

Yu, H., Liu, Y., Harrington, R.M. and Lamontagne, M. 2016. Seismicity along St. Lawrence Paleorift faults overprinted by a meteorite impact structure in Charlevoix, Québec, Eastern Canada. *Bulletin of the Seismological Society of America*, 106(6):2663-2673.